

A solution to the Kelvin wake angle controversy

Alexandre Darmon,^{1,2,*} Michael Benzaquen,^{1,*} and Elie Raphaël¹

¹*PCT, UMR CNRS 7083 Gulliver, ESPCI, Paris, France*

²*EC2M, UMR CNRS 7083 Gulliver, ESPCI, Paris, France*

(Dated: October 1, 2013)

Gravity waves generated by an object moving at constant speed at the water surface form a specific pattern commonly known as the Kelvin wake. It was proved by Lord Kelvin that such a wake is delimited by a constant angle $\simeq 19.47^\circ$. However a recent study by Rabaud and Moisy based on the observation of airborne images showed that the wake angle seems to decrease as the Froude number Fr increases, scaling as Fr^{-1} for large Froude numbers. To explain such observations the authors make the strong hypothesis that an object of size b cannot generate wavelengths larger than b thus leading to unrealistic pressure fields to model the object. With no need of such an assumption, we here analytically show that the angle corresponding to the maximum amplitude of the waves scales as Fr^{-1} for large Froude numbers whereas the angle delimiting the wake region outside which the surface is essentially flat remains constant and equal to the Kelvin angle for all Fr .

PACS numbers: 47.35.Bb ; 92.10.hh ; 47.15.Tr ; 02.70.Ns

Simply by looking at a duck swimming in a pond or a cargo ship moving on a calm sea, one can clearly tell that there is something common about their wake. Indeed, they both display a familiar V-shaped pattern which only differ from one another by their dimensions. In 1887, Lord Kelvin [1] showed that the wake created by an object moving at a uniform pace is always delimited by an angle equal to $\arcsin 1/3 = 19.47^\circ$. This theory, based on stationary phase arguments, is widely used both at theoretical and technical levels [2–5]. Since Lord Kelvin, other studies have shown that two sets of waves can be distinguished in the wake: the so-called transverse waves and diverging waves [6, 7]. Their amplitudes directly depend on the Froude number $Fr = V/\sqrt{gb}$, where V is the speed of the moving object and b its length [8]. It has been observed that as the Froude number increases, so does the amplitude of the diverging waves; but that of the transverse waves decreases rapidly and seems to vanish for sufficiently high Froude numbers [2]. Speedboats, whose range of reachable Froude number is large, typically until $Fr \simeq 3$, experience different regimes as the Froude number is increased, eventually entering the so-called planing regime in which their drag is significantly decreased as they displace fewer quantities of water [9–11]. The understanding of the wave drag is of great practical importance in the ship industry for the hull design [12–14]. At smaller scales, the wave drag for capillary gravity waves has also been studied extensively [15–17] and is notably of interest for insect locomotion [18].

Recent experimental observations by Rabaud and Moisy have challenged the commonly accepted theory of Lord Kelvin [19]. Based on airborne observations of ship wakes, the authors show that the wake angle seems to decrease as the Froude number is increased, scaling as Fr^{-1} for large Froude numbers. To explain their observations, they make the strong hypothesis that an object of

size b cannot generate wavelengths greater than b . Even though this assumption leads to consistent results, it is not justified and in particular leads to unrealistic pressure fields to model the object. These results have raised the attention of the community and have been subjected to questioning [20, 21].

We here propose an explanation of such observations with no need of the maximum wavelength argument. We first perform numerical evaluation of the surface displacement induced by a moving pressure field of typical size b above the surface of water and show that two angles can actually be highlighted in the wake: the outer angle delimiting the wake, shown to be constant and equal to the Kelvin angle, and an inner angle corresponding to the maximum amplitude of the waves. We then analytically prove that the latter is not constant and scales as Fr^{-1} at large Froude numbers.

In the pure gravity waves limit, the surface displacement generated by a pressure field $p(x, y)$ moving in the $-x$ direction with constant speed V can be written in the frame of reference of the moving perturbation as [22, 23]:

$$\zeta(x, y) = - \lim_{\varepsilon \rightarrow 0} \iint \frac{dk d\theta}{4\pi^2 \rho} \frac{\hat{p}(k, \theta) e^{-ik(\cos \theta x - \sin \theta y)}}{c(k)^2 - V^2 \cos^2 \theta + 2i\varepsilon V \cos \theta/k}, \quad (1)$$

where $\hat{p}(k, \theta)$ is the Fourier Transform of $p(x, y)$ in cylindrical coordinates, ρ is the water density and $c(k) = (g/k)^{1/2}$ is the phase speed for pure gravity waves. Let us now nondimensionalize the problem through:

$$Z = \frac{4\pi^2 \zeta}{b}; \quad X = \frac{x}{b}; \quad Y = \frac{y}{b}; \quad K = kb; \quad (2a)$$

$$\hat{P} = \frac{\hat{p}}{\rho g b^3}; \quad \tilde{\varepsilon} = \frac{\varepsilon}{\sqrt{g/b}}, \quad (2b)$$

where b is the typical size of the pressure field $p(x, y)$.

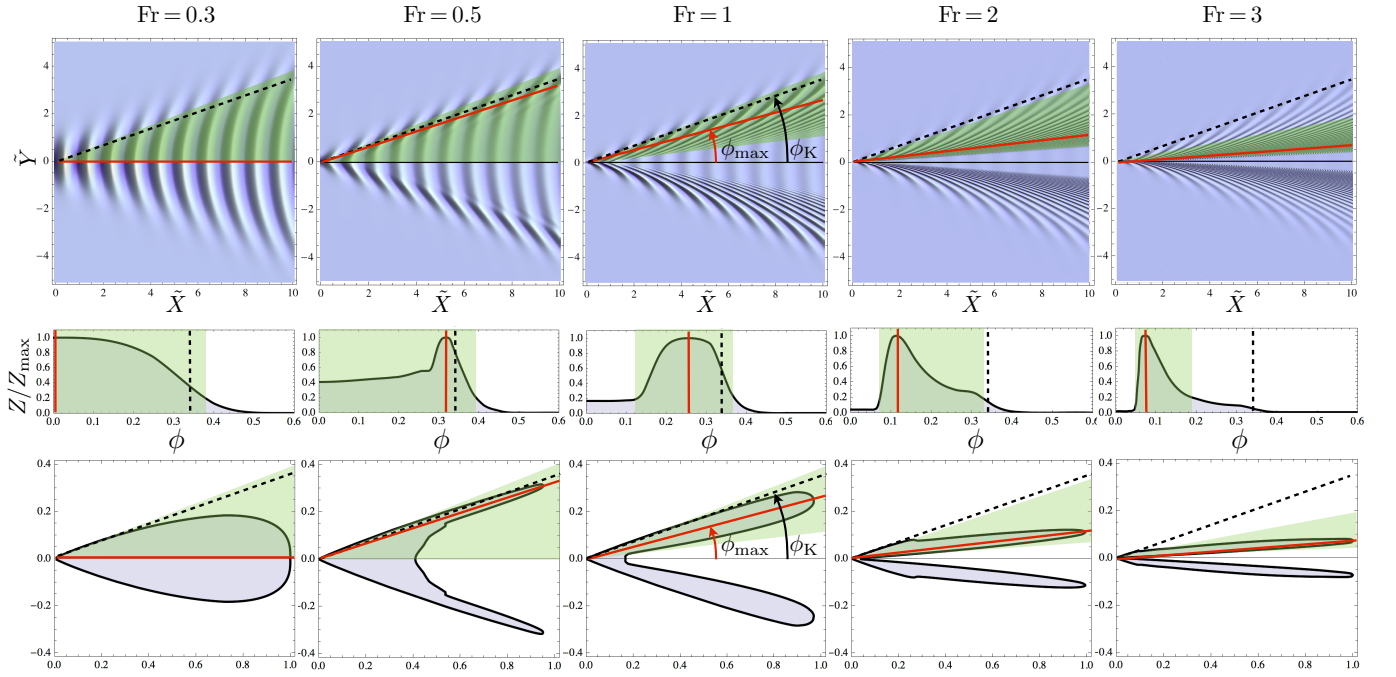


FIG. 1. Color online. 1st row: Relief plots of the surface displacement computed using Eq. (8) for different Froude numbers as a function of $\tilde{X} = X/\Lambda$ and $\tilde{Y} = Y/\Lambda$ where $\Lambda = 2\pi\text{Fr}^2$ is the dimensionless wavelength. 2nd row: Plot of the normalized angular envelope of the surface displacement as a function of ϕ for different Froude numbers where ϕ is the polar angle originating at the horizontal axis. The angular envelope was calculated by interpolating the maxima of the waves amplitudes over one wavelength sufficiently far from the perturbation. 3rd row: Polar plot of the normalized angular envelope as defined in the 2nd row for different Froude numbers. In all graphs the maximum of the angular envelope obtained for $\phi = \phi_{\max}$ is signified with a solid red line and the Kelvin angle $\phi_K = \arcsin(1/3)$ is represented by a dashed black line. The green colored region delimits the area in which the amplitude of the waves is above 20% of the maximum of the angular envelope.

Equation (1) together with Eq. (2) becomes:

$$Z(X, Y) = \int_{-\pi}^{\pi} d\theta F(\theta, X, Y), \quad (3)$$

where:

$$F(\theta, X, Y) = -\lim_{\varepsilon \rightarrow 0} \int_0^{\infty} K dK \frac{\hat{P}(K, \theta) e^{-iK(\cos\theta X - \sin\theta Y)}}{1 - \text{Fr}^2 K \cos^2\theta + 2i\varepsilon\text{Fr} \cos\theta}. \quad (4)$$

Using the Sokhotski-Plemelj formula (see e.g. [24]), one can write:

$$F(\theta, X, Y) = i\pi\Phi(K_0, \theta, X, Y) + G(\theta, X, Y), \quad (5)$$

where:

$$\Phi(K, \theta, X, Y) = \frac{K \hat{P}(K, \theta) e^{-iK(\cos\theta X - \sin\theta Y)}}{\text{Fr}^2 \cos^2\theta}, \quad (6)$$

$$K_0(\theta) = \frac{1}{\text{Fr}^2 \cos^2\theta}, \quad (7)$$

and $\int d\theta G(\theta, X, Y)$ is a rapidly decreasing function with the distance to the perturbation. According to Eqs. (3), (5), (6) and (7) and sufficiently far from the perturbation,

the surface displacement is well approximated by:

$$Z(X, Y) \simeq i\pi \int_{-\pi}^{\pi} d\theta \frac{\hat{P}(K_0(\theta), \theta) e^{-i(\cos\theta X - \sin\theta Y)/(\text{Fr}^2 \cos^2\theta)}}{\text{Fr}^4 \cos^4\theta}. \quad (8)$$

For a given pressure distribution one can thus obtain the surface displacement by numerically evaluating the integral in Eq. (8).

Considering a Gaussian pressure field of typical size b , symmetrical around the origin, with corresponding Fourier transform of the form:

$$\hat{P}(K) = \exp[-K^2/(4\pi^2)], \quad (9)$$

Eq. (8) yields the profiles displayed in Fig. 1. The first row shows relief plots of the surface displacement computed using Eq. (8) for different Froude numbers as a function of $\tilde{X} = X/\Lambda$ and $\tilde{Y} = Y/\Lambda$ where $\Lambda = 2\pi\text{Fr}^2$ is the dimensionless wavelength. The second row displays the normalized angular envelope of the surface displacement as a function of ϕ for different Froude numbers where ϕ is the polar angle originating at the horizontal axis. The angular envelope was calculated by interpolating the maxima of the waves amplitudes over one wavelength sufficiently far from the perturbation. The third

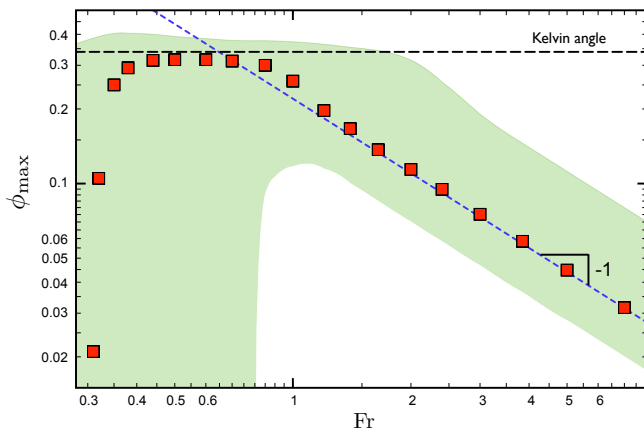


FIG. 2. Color online. Plot of ϕ_{\max} as defined in paragraph 2. as a function of the Froude number (red squares). The green colored region delimits the area in which the amplitude of the waves is above 20% of the maximum of the angular envelope as defined in paragraph 2. The dashed black line signifies the Kelvin angle $\phi_K = \arcsin(1/3)$. The dashed blue line represents the asymptotic theoretical prediction at large Froude numbers as given by Eq. (18).

row displays polar plots of the normalized angular envelope as defined in the second row for different Froude numbers. In all graphs the maximum of the angular envelope obtained for $\phi = \phi_{\max}$ is signified with a solid red line and the Kelvin angle $\phi_K = \arcsin(1/3)$ is represented by a dashed black line. The green colored region delimits the area in which the amplitude of the waves is above 20% of the maximum of the angular envelope. We chose this as an arbitrary criteria for what the eye can see. It somehow sets the error bars to the angle determined by just looking at a boat's wake on an airborne picture. Firstly, as one can see, the wake pattern strongly depends on the Froude number. At $Fr = 0.5$ one can clearly distinguish two different sets of waves: the so-called transverse waves that are orthogonal to the trajectory, and the so called diverging waves that are located at the edges of the wake. As the Froude number is increased the relative amplitude of the transverse waves decreases until vanishing making way for the diverging waves. Secondly, we are interested in the evolution of ϕ_{\max} as the Froude number increases. Fig. 2 displays ϕ_{\max} as a function of the Froude number (red squares). The green colored region has the same meaning as that of Fig. 1. The dashed black line signifies the Kelvin angle $\phi_K = \arcsin(1/3)$. The dashed blue line represents the asymptotic scaling Fr^{-1} . At $Fr = 0.3$ and below, the maximum of the wake's angular envelope is located at the central line $\phi = 0$. A continuous transition in which the maximum is displaced to the edges of the wake $\phi_{\max} \simeq \phi_K$ is observed at $Fr \simeq 0.31$. The angle ϕ_{\max} then remains constant until $Fr \simeq 0.7$ before it starts to decrease eventually scaling as Fr^{-1} . As one

can see in Fig. 2 the green beam also scales as Fr^{-1} for large Froude numbers thus explaining the observations of Rabaud and Moisy [19]. Thirdly, the waves are always confined within the Kelvin wake and always reach its outer boundary (see Fig. 1), even though the relatively small amplitude around this region makes it difficult to see on photographs as it might be diluted in the noise of the open sea.

In the following we demonstrate analytically the $\phi_{\max} \sim Fr^{-1}$ scaling for large Froude numbers. Surface displacement as given by Eq. (8) can be expressed in polar coordinates $X = R \cos \phi$, $Y = R \sin \phi$ as:

$$\check{Z}(R, \phi) \simeq i\pi \int_{-\pi}^{\pi} d\theta \frac{\hat{P}(K_0(\theta), \theta) e^{-iR \cos(\theta+\phi)/(Fr^2 \cos^2 \theta)}}{Fr^4 \cos^4 \theta}. \quad (10)$$

The integral in Eq. (10) is of the form $\int d\theta f(\theta) e^{ig(\theta)}$ and may be approximated through the method of the steepest descent [24]. For $R/Fr^2 > 1$, the integrand oscillates rapidly and there are two stationary points given by $g'(\theta) = 0$:

$$\theta_1(\phi) = \frac{1}{2}(\arcsin(3 \sin \phi) - \phi), \quad (11a)$$

$$\theta_2(\phi) = \frac{1}{2}(\pi - \arcsin(3 \sin \phi) - \phi). \quad (11b)$$

One shall note that at the Kelvin angle $\phi = \phi_K = \arcsin(1/3)$, the two points θ_1 and θ_2 coalesce and thus the saddle-point method won't be accurate in the vicinity of $\phi = \phi_K$. The calculation for two coalescing saddle points [25] won't be developed it here as our aim is to study the behavior of ϕ_{\max} at large Froude numbers for which *a priori* ϕ_{\max} is far below ϕ_K . In this range both saddle points can safely be considered independently. Hence, far below ϕ_K one can write:

$$\check{Z}(R, \phi) \simeq i\pi \left(\check{Z}_1(R, \phi) + \check{Z}_2(R, \phi) \right), \quad (12)$$

where:

$$\check{Z}_j(R, \phi) = \sqrt{\frac{2\pi}{|\partial_\theta^2 g(R, \theta_j, \phi)|}} f(\theta_j) e^{i(g(R, \theta_j, \phi) + \frac{\pi}{4})}, \quad (13)$$

where θ_j , $j \in \{1, 2\}$, are implicit function of ϕ as defined through Eq. (11) and where:

$$f(\theta) = \frac{\hat{P}(K_0(\theta), \theta)}{Fr^4 \cos^4 \theta}, \quad (14)$$

$$g(R, \theta, \phi) = -\frac{R \cos(\theta + \phi)}{Fr^2 \cos^2 \theta}. \quad (15)$$

One can easily check that far below ϕ_K the function \check{Z}_1 exclusively defines the transverse waves whereas \check{Z}_2 exclusively defines the diverging waves. Let us again take

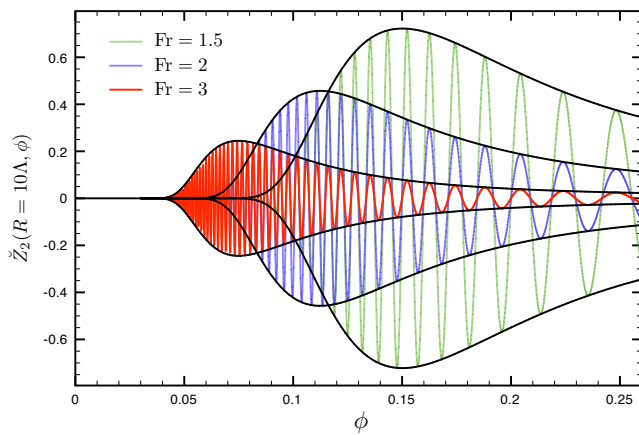


FIG. 3. Color online. Plot of $\check{Z}_2(R = 10\Lambda, \phi)$ as given by Eq. (13) with the Gaussian pressure field of Eq. (9) where $\Lambda = 2\pi\text{Fr}^2$ as a function of ϕ for different Froude numbers. Their angular envelopes given by Eq. (16) are signified with a solid black line.

the Gaussian pressure field of Eq. (9). As an effect of the normalization of the pressure field, both functions decrease as the Froude number is increased. Yet, the amplitude of the \check{Z}_1 waves scales as Fr^{-4} whereas the amplitude of the \check{Z}_2 waves scales as $\text{Fr}^{-3/2}$ thus decreasing slower. This explains why the transverse waves vanish as compared to the diverging waves for large Froude numbers. Let us now thus focus on the \check{Z}_2 function. At a given R , the angular envelope function of \check{Z}_2 is given by:

$$h(R, \phi) = \sqrt{\frac{2\pi}{|\partial_{\theta_2}^2 g(R, \theta_2, \phi)|}} f(\theta_2), \quad (16)$$

where θ_2 and g are defined through Eqs. (11) and (15). Figure 3 displays $\check{Z}_2(R = 10\Lambda, \phi)$ as a function of ϕ for different Froude numbers. Their angular envelopes given by Eq. (16) are signified with a solid black line. For small angles ϕ , Eq. (16) reduces to:

$$h(R, \phi) \simeq \sqrt{\frac{\pi}{16R}} \frac{1}{\text{Fr}^3 \phi^{5/2}} \exp\left[-\frac{1}{64\pi^2 \text{Fr}^4 \phi^4}\right]. \quad (17)$$

The maximum of this function is obtained at $40\pi^2 \text{Fr}^4 \phi_{\max}^4 = 1$ which yields:

$$\phi_{\max} = \frac{1}{40^{1/4} \sqrt{\pi}} \frac{1}{\text{Fr}}. \quad (18)$$

As one can see on Fig. 2, this prediction (blue line) fits perfectly the numerical results at large Froude numbers. Note that the numerical prefactor in Eq. (18) may depend on the precise form of the pressure distribution.

In this paper we provided a solution to the recent wake angle controversy [19–21]. We showed that the angle delimiting the wake region outside which the surface is unperturbed remains constant and equal to the Kelvin angle

for all Froude numbers. However a different angle corresponding to the maximum of the amplitude of the waves can indeed be identified. With no need of unphysical pressure fields we showed that this angle scales as Fr^{-1} for large Froude numbers thus behaving as a Mach angle, as highlighted by Rabaud and Moisy. Note that the observation of the Kelvin angle at large Froude numbers can be made difficult because of the small amplitude of the waves on the edges of the wake. We wish to thank V. Bacot, T. Salez and O. Dauchot for fruitful discussions.

* These authors contributed equally to this work.

- [1] L. Kelvin, Proc. R. Soc. London, Ser. A **42**, 80 (1887).
- [2] J. Lighthill, *Waves in Fluids* (Cambridge University Press, Cambridge, 1978).
- [3] H. Lamb, *Hydrodynamics* (Cambridge University Press, Cambridge, 6th ed, 1993).
- [4] O. Darrigol, *Words of Flow: A History of Hydrodynamics from the Bernoullis to Prandtl* (Oxford University, New York, 1978).
- [5] K. E. Parnell and H. Kofoed-Hansen, Coastal Management **29**, 217 (2001).
- [6] F. Crawford, Am. J. Phys. **52**, 782 (1984).
- [7] D. E. Nakos and P. D. Sclavounos, J. Fluid Mech. **215**, 263 (1990).
- [8] The Froude number considered here is the hull Froude number.
- [9] E. Cumbertach, J. Fluid Mech. **4**, 466 (1958).
- [10] E. M. Casling, Journal of Engineering Mathematics **12**, 43 (1978).
- [11] C. Lai and A. Troesch, Journal of Ship Research **39**, 1 (1995).
- [12] E. O. Tuck, D. C. Scullen, and L. Lazauskas, 24th Symposium on Naval Hydrodynamics, Fukuoka, Japan (8-13 July 2002).
- [13] K. Suzuki, Y. Nakata, M. Ikehata, and H. Kai, Fourth Int. Conf. on Fast Sea Transportation, Sydney (21-23 July 1997).
- [14] M. Rabaud and F. Moisy, Innov-Sail, Lorient (26-28 June 2013).
- [15] M. Benzaquen, F. Chevy, and E. Raphaël, Europhys. Lett. **96**, 34003 (2011).
- [16] M. Benzaquen and E. Raphaël, Europhys. Lett. **97**, 14007 (2012).
- [17] M. Le Merrer, C. Clanet, D. Quéré, E. Raphaël, and F. Chevy, Proc. Natl. Acad. Sci **108(30)**, 1506415068 (2011).
- [18] A. D. Chepelianskii, F. Chevy, and E. Raphaël, Phys. Rev. Lett. **100**, 074504 (2008).
- [19] M. Rabaud and F. Moisy, Phys. Rev. Lett **110**, 214503 (2013).
- [20] B. Verberck, Nature Phys. **9**, 390 (2013).
- [21] A. Cho, Science Now **9**, 2013 (2013).
- [22] T. H. Havelock, Proc. R. Soc. A **95**, 354 (1908).
- [23] E. Raphaël and P.-G. de Gennes, Phys. Rev. E **53**, 3448 (1996).
- [24] W. Appel, *Mathematics for Physics and Physicists* (Princeton University Press, 2007).
- [25] R. S. Johnson, *A Modern Introduction to the Mathemati-*

cal Theory of Water Waves (Cambridge University Press, 1997).